



## On the soot combustion mechanism using 3DOM ceria catalysts

Virginia Alcalde-Santiago, Arantxa Davó-Quiñonero, Dolores Lozano-Castelló,  
Agustín Bueno-López\*

Department of Inorganic Chemistry, University of Alicante, Carretera de San Vicente s/n. E03080, Alicante, Spain



### ARTICLE INFO

**Keywords:**

Soot  
Ceria  
3DOM  
Active oxygen  
NO<sub>x</sub>  
Diesel

### ABSTRACT

CeO<sub>2</sub> catalysts have been prepared with conventional (Ref) and three dimensionally ordered macroporous (3DOM) structures, and the effect of the structure on the soot combustion mechanism has been studied in detail. Isotopic exchange experiments showed that the CeO<sub>2</sub>-3DOM catalyst produces more active oxygen upon O<sub>2</sub> chemisorption than the counterpart CeO<sub>2</sub>-Ref catalyst, and this active oxygen is transferred more efficiently to soot due to the macroporous structure. CeO<sub>2</sub>-3DOM and CeO<sub>2</sub>-Ref also accelerate the oxidation of NO to NO<sub>2</sub>, and their activity is equal. However, CeO<sub>2</sub>-3DOM utilizes NO<sub>2</sub> more efficiently than CeO<sub>2</sub>-Ref for soot combustion. NO<sub>2</sub> has two roles in the soot combustion mechanism: i) reacts with soot and ii) is chemisorbed on ceria and produces active oxygen, which is more oxidizing than NO<sub>2</sub>. In ceria catalysts with a conventional structure, the main role of NO<sub>2</sub> is the direct oxidation of soot, because active oxygen has restrictions to be transferred from catalyst to soot due to the poor soot-catalyst solid-solid contact. However, the 3DOM structure improves the transfer of active oxygen, and therefore, an additional benefit is obtained from NO<sub>2</sub>, that is, NO<sub>2</sub> contributes to active oxygen production and the 3DOM structure allows its efficient transference to soot.

### 1. Introduction

Cerium oxide is a good catalyst to accelerate soot combustion and control gas pollution in diesel vehicles [1–6]. This oxide has a long history of success in three way catalysts (TWC) used in gasoline vehicles [7–9]. Cerium oxide is able to store oxygen from the gas phase and release this oxygen when required, because it is able to adapt the cerium/oxygen atomic ratio in the ceria lattice depending on the gas composition. This well-known feature of cerium oxide used in TWC to buffer the oxidizing/reducing conditions is also useful to accelerate diesel soot combustion. It has been demonstrated by isotopic experiments [1,10] that cerium oxide exchanges oxygen atoms with O<sub>2</sub>, which is one of the main oxidizing gases in diesel exhausts together with NO<sub>2</sub>. The dynamic equilibrium between ceria oxygen and the oxygen-containing gas molecules leads to the formation of oxygen radicals, which are intermediate species of the oxygen exchange processes. These oxygen radicals are usually referred to as “active oxygen” [11,12], because they are highly oxidizing and are very efficient for soot combustion. Some authors have related active oxygen with the presence of peroxide and/or super oxide species on the ceria surface [11].

In addition to the active oxygen soot combustion mechanism, ceria also accelerates soot combustion by the so-called “NO<sub>2</sub>-assisted mechanism” [13]. NO is the main nitrogen oxide emitted by diesel engines,

and ceria accelerates the NO + O<sub>2</sub> reaction to yield NO<sub>2</sub>. NO<sub>2</sub> is more oxidizing than NO and O<sub>2</sub> and reacts rapidly with soot at lower temperature than O<sub>2</sub> and NO.

Both the active oxygen and the NO<sub>2</sub>-assisted soot combustion mechanisms have strong and weak points. Active oxygen species are more oxidizing than NO<sub>2</sub>, but their lifetime is very short and most active oxygen species are depleted yielding stable gas molecules before they reach the soot particles. One of the main handicaps of the active oxygen mechanism is that both catalyst and soot are solids, and the solid-solid contact is poor. This limits the utilization of active oxygen, because the transfer of active oxygen from ceria particles to soot is limited to few contact points. On the contrary, NO<sub>2</sub> is a stable molecule that is able to travel in the gas phase from catalyst to soot, but it is less oxidizing than active oxygen.

The active oxygen and NO<sub>2</sub>-assisted soot combustion mechanisms take place simultaneously during the ceria-catalyzed soot combustion in gas streams with NO<sub>x</sub> + O<sub>2</sub>, like those in real diesel exhausts. The contribution of each mechanism to the global soot combustion depends on the particular reaction conditions, that is, physical-chemical properties of the ceria catalyst, soot-catalyst contact, gases concentrations, etc. Since active oxygen is more oxidizing than NO<sub>2</sub>, it would be desirable to maximize the participation of active oxygen to the global combustion of soot. It has been demonstrated that an optimized ceria

\* Corresponding author.

E-mail address: agus@ua.es (A. Bueno-López).

catalyst using active oxygen very efficiently is able to outperform the behavior of a commercial Pt catalyst, which only oxidizes soot throughout the NO<sub>2</sub>-assisted mechanism [14].

Important efforts are being done to improve soot combustion ceria catalysts in order to maximize the utilization of the active oxygen mechanism. One strategy is to improve the production of active oxygen by modifying ceria with dopants [15–18], and the other one is to prepare ceria particles with controlled morphology [14,19,20] to improve the transfer of active oxygen from catalyst to soot. For instance, high surface area ceria nanoparticles transfer active oxygen very efficiently to soot [14].

It has been recently reported the high catalytic activity for soot combustion of three dimensionally ordered macroporous (3DOM) ceria. This high activity has been attributed to the improved soot-catalyst contact due to the macroporous structure [21,22]. In our opinion, this is one of the most relevant advances of the recent years in the development of soot combustion catalysts, but the effect of the macroporous structure in the soot combustion mechanism has not been studied in detail. We believe that understanding the mechanisms taking place during the 3DOM ceria-catalyzed soot combustion is necessary to focus the further design and optimization of these promising catalysts.

The goal of the current study is to analyze the participation of the active oxygen and NO<sub>2</sub>-assisted soot combustion mechanisms using 3DOM ceria catalysts. 3DOM ceria has been prepared, both pure and doped with copper to enhance the oxidation of NO to NO<sub>2</sub>, and tested for soot combustion in O<sub>2</sub>/N<sub>2</sub> and NO<sub>x</sub>+O<sub>2</sub>/N<sub>2</sub>. Their catalytic behavior has been compared with that of two counterpart catalysts without 3DOM structure. Isotopic exchange experiments have been carried out to analyze the active oxygen formation capacity of each catalyst, and all catalysts have been characterized in detail.

## 2. Experimental details

### 2.1. Catalysts preparation

Four catalysts were prepared, which are referred to as CeO<sub>2</sub>-Ref, CeO<sub>2</sub>-3DOM Cu/CeO<sub>2</sub>-Ref and Cu/CeO<sub>2</sub>-3DOM.

For the preparation of CeO<sub>2</sub>-3DOM, a colloidal crystal template of monodisperse spheres of polymethylmethacrylate (PMMA) was synthesized. This template was prepared by polymerization of methylmethacrylate, methacrylic acid, and divinylbenzene (100:1:5 vol ratio) in boiling aqueous solution (H<sub>2</sub>O/methylmethacrylate volume ratio 4:1) for 75 min, and the polymerization reaction was initiated with K<sub>2</sub>S<sub>2</sub>O<sub>8</sub> (0.8 mg/L). All these reactants were purchased from Sigma-Aldrich. After cooling, colloidal crystals were obtained by centrifugation of the monodispersed spheres at 5000 rpm for 60 min.

Ce(NO<sub>3</sub>)<sub>3</sub>·6H<sub>2</sub>O (Aldrich, 99%) was dissolved in ethanol, and citric acid was added to the solution in an equimolar proportion to the Ce<sup>3+</sup> content. This solution was added dropwise to the PMMA template, and the excess was removed under soft vacuum. After drying at 60 °C the impregnation was repeated, and the PMMA template was finally removed by calcination at 600 °C for 6 h. The reference catalyst (CeO<sub>2</sub>-Ref) was prepared following the same protocol but without impregnation into the PMMA template, that is, the solution with citric acid and the Ce precursor was directly dried and calcined.

The copper-containing catalysts were prepared by excess solvent impregnation of the ceria supports with an ethanol solution of Cu(NO<sub>3</sub>)<sub>2</sub>·2.5H<sub>2</sub>O (Sigma-Aldrich, 99.99%). After drying at 80 °C overnight, the catalysts were calcined at 500 °C for 2 h. The target copper loading was 2 wt.%.

### 2.2. Catalysts characterization

SEM images were obtained in a Field Emission Scanning Electron Microscope (FESEM) Merlin VP Compact from Zeiss, working at very low voltages (from 0.02 kV to 30 kV) to minimize charging effects.

The composition of the catalysts was determined by Micro-XRF in an Orbis Micro-XRF Analyzer from EDAX. Areas of 300 μm in diameter were analyzed and three different spots were measured and averaged to obtain the composition of each catalyst.

The porosity of catalysts was characterized by N<sub>2</sub> adsorption, mercury intrusion porosimetry and Helium density. N<sub>2</sub> adsorption-desorption isotherms were measured at –196 °C in an automatic volumetric system (Autosorb-6, Quantachrome) after degassing the catalysts at 150 °C for 2 h under vacuum. The macroporosity of the catalysts was studied by mercury porosimetry in a Poremaster 60 GT (Quantachrome). The powdered catalysts were outgassed in this case at 50 °C under vacuum for 12 h. The closed porosity was studied by helium pycnometry using an automatic helium pycnometer MicroUltrapyc 1200e (Quantachrome).

A dispersive Raman Jasco NRS-5100 Spectrometer with a He-Ne laser source (632.8 nm) was used for Raman spectroscopy characterization. 2 scans obtained with 1.8 mW laser power were averaged to obtain each spectrum.

X-ray diffractograms were recorded in a Rigaku Miniflex II diffractometer, using CuK<sub>α</sub> radiation ( $\lambda = 0.15418$  nm). Diffractograms were registered between 10 and 90° (2θ) with a step of 0.025°. The average crystal sizes (D) were determined using the equations of Scherrer and Williamson-Hall:

$$D = \frac{K \cdot \lambda}{\beta \cdot \cos \theta} \text{ Scherrer's equation}$$

where  $\lambda$  is the wavelength of the X-ray radiation ( $\lambda = 0.15418$  nm for CuK<sub>α</sub>),  $\beta$  is the full width at half maximum of the diffraction peak considered (111), K is a shape factor, which is taken as 0.9 (1 being a perfect sphere) and  $\theta$  is the diffraction angle at which the (111) peak appears.

The estimation of crystal size of doped oxides presents some problems, because the introduction of foreign cations within the ceria lattice deforms the structure and affects the  $\beta$  values, and the insertion of copper cations into the ceria lattice cannot be ruled out in advance. The Williamson-Hall's equation separates the effects of size and strain in the crystals, and is more convenient for the estimation of crystal size of mixed oxides:

$$\beta_{\text{Total}} = \beta_{\text{Size}} + \beta_{\text{Strain}} = \frac{0.9 \cdot \lambda}{D \cdot \cos \theta} + \frac{4 \cdot (\Delta d) \cdot \sin \theta}{d \cdot \cos \theta} \text{ Williamson-Hall' s equation}$$

where  $\beta_{\text{Total}}$  is the full width half maximum of the XRD peak and  $\Delta d$  is the difference of the  $d$  spacing corresponding to a typical peak. A plot of  $\beta_{\text{Total}} \cdot \cos \theta$  against  $4 \cdot \sin \theta$  yields the average crystal size from the intercept value.

The amount of copper cations incorporated into the ceria lattice in the copper-containing catalysts was estimated from the XRD patterns using the Kim's equation [23,24].

$$CP_{\text{Cu-Ce}} = CP_{\text{Ce}} + (0.0220 \cdot (rCu^{2+} - rCe^{4+}) + 0.00015 \cdot (ZCu^{2+} - ZCe^{4+})) \cdot mCu^{2+}$$

Kim's equation, where

$CP_{\text{Cu-Ce}}$  is the cell parameter of copper-doped ceria,

$CP_{\text{Ce}}$  is the cell parameter of pure ceria

$rCu^{2+}$  and  $rCe^{4+}$  are the cationic radii of Cu<sup>2+</sup> and Ce<sup>4+</sup>, respectively,

$ZCu^{2+}$  and  $ZCe^{4+}$  are the charges of the Cu<sup>2+</sup> and Ce<sup>4+</sup> cations, respectively, and

$mCu^{2+}$  is the fraction of copper loaded into the ceria lattice.

Temperature programmed reduction experiments were carried out with H<sub>2</sub> (H<sub>2</sub>-TPR) in a thermobalance (Mettler Toledo; TGA/SDTA851) coupled to a mass spectrometer (Pfeiffer Vacuum; Thermostar GSD301T). The catalysts (20 mg) were heated in 5% H<sub>2</sub>/Ar (40 ml/min) at 10 °C/min from room temperature until 900 °C.

XPS characterization was carried out in a K-ALPHA Thermo Scientific device, using Al-K $\alpha$  radiation (1486.6 eV). The X-ray spot was focussed on the catalysts with a diameter of 400  $\mu\text{m}$ , at 3 mA  $\times$  12 kV. The binding energy scale was adjusted by setting the C1s transition at 284.6 eV.

### 2.3. Catalytic tests

Catalytic experiments were carried out in a tubular quartz reactor following the gas concentration with Specific NDIR-UV gas analyzers for CO, CO<sub>2</sub>, NO, NO<sub>2</sub> and O<sub>2</sub> (Fisher-Rosemount, models BINOS 100, 1001 and 1004). The temperature was raised from room temperature until 700 °C at 10 °C/min. Two gas mixtures were used (500 ml/min; GHSV = 30,000 h<sup>-1</sup>): 5% O<sub>2</sub>/N<sub>2</sub> and 500 ppm NO/5% O<sub>2</sub>/N<sub>2</sub>, and experiments were performed only with the catalysts and with soot-catalysts mixtures (20 mg of soot + 80 mg of catalyst + 300 g SiC) prepared with a spatula in the so-called loose contact mode in order to obtain results with practical meaning [25]. The model soot used was a carbon black by Evonik-Degussa GmbH (Printex U).

### 2.4. Isotopic exchange experiments

Isotopic exchange experiments were carried out with <sup>18</sup>O<sub>2</sub>. The experimental set-up consisted of a mass flow controller for the carrier gas (0.1 ml/min sensitivity), an injection valve with a 100  $\mu\text{l}$  loop, and two high sensitivity pressure transducers, which allow gas injections without pressure variation in the system. The gas composition was monitored with a mass spectrometer Pfeiffer Vacuum (model OmniStar), operating at 1 s frequency. The experiments were carried out in a 5 mm inner diameter cylindrical fixed-bed reactor with 80 mg of catalyst diluted with 300 mg of SiC and packed between plugs of quartz wool. The catalysts were heated at 450 °C under 10 ml/min of He until the CO<sub>2</sub> (*m/z* 44) and H<sub>2</sub>O (*m/z* 18) signals recovered the baseline level. Then, several pulses of Ar (100  $\mu\text{l}$  and 9 psi) were feed to confirm reproducibility and a pulse of <sup>18</sup>O<sub>2</sub> (Isotec, 99%; 100  $\mu\text{l}$  and 9 psi) was finally feed.

## 3. Results and discussion

### 3.1. Catalysts porosity characterization by FESEM, N<sub>2</sub> adsorption-desorption, He density and mercury intrusion porosimetry

Representative FESEM images of the CeO<sub>2</sub>-3DOM and CeO<sub>2</sub>-Ref catalysts are shown in Fig. 1, where important morphological differences are noticed.

A sponge-like structure is distinguished in the 3DOM catalyst shown in Fig. 1a, where the open porosity left upon removal of the PMMA template is preserved. On the contrary, the catalyst prepared without template (Fig. 1b) shows a bulky particle.

These morphological differences strongly affect the porosity of the catalysts, which has been characterized by N<sub>2</sub> adsorption-desorption, mercury intrusion porosimetry and He density measurements. Fig. 2 shows the N<sub>2</sub> adsorption-desorption isotherms and Table 1 the BET specific surface areas calculated from these isotherms. The pore size distributions determined from N<sub>2</sub> isotherms using the BJH method are included in the Supplementary Material file (Fig. S2).

All catalysts present few N<sub>2</sub> adsorption at very low relative pressures and an hysteresis loop at intermediate or high relative pressures, that is, the microporosity is low in these materials and they present meso and/or macropores. Note that the porosity of the “Ref” samples can be mainly attributed to the space left by the crystals packed forming the catalyst particles, and the first monolayer of N<sub>2</sub> is adsorbed on the surface the primary crystals [26]. The 3DOM samples, additionally, have porosity created by removal of the PMMA template.

The shape of the hysteresis loops in CeO<sub>2</sub>-Ref and Cu/CeO<sub>2</sub>-Ref suggests the presence of mesopores, with the loops appearing above 0.4

relative pressure. The BET surface areas of these two materials are 23 and 21 m<sup>2</sup>/g, respectively.

On the contrary, the hysteresis loop of Cu/CeO<sub>2</sub>-3DOM starts at 0.8 relative pressure and last points of the isotherm rise rapidly, which is most likely due to the presence of macropores. The isotherm of CeO<sub>2</sub>-3DOM is qualitatively similar to that of Cu/CeO<sub>2</sub>-3DOM, but the hysteresis loop is clearly smaller for the copper-free catalyst, suggesting the presence of a lower amount of macropores. The BET surface areas of these two materials are consistent with the lower porosity in CeO<sub>2</sub>-3DOM (12 m<sup>2</sup>/g) with regard to Cu/CeO<sub>2</sub>-3DOM (21 m<sup>2</sup>/g). As it will be demonstrated afterwards, part of the macroporosity created on CeO<sub>2</sub>-3DOM after removal of the PMMA template remains closed due to the accumulation of carbonates, and part of these carbonates are removed after copper impregnation. This removal of carbonates is attributed to the slightly acid pH of the copper nitrate solution used for copper impregnation. It was experimentally measured that the pH of this solution is 5.5, and this would favor the release of CO<sub>2</sub> chemisorbed on the solid.

This hypothesis is supported by the He density values compiled in Table 1. The expected He density for bulk ceria is 7.2 g/cm<sup>3</sup> [27]. The copper-containing catalysts reach this density (7.1–7.2 g/cm<sup>3</sup>), but the supports present slightly lower values (6.9 g/cm<sup>3</sup>). This is attributed to the presence of closed porosity that is not accessible neither for He in density measurements nor for N<sub>2</sub> during adsorption-desorption at 196 °C, and that gets open after copper loading.

The macroporosity of the samples was characterized by mercury intrusion porosimetry, and the pore size distributions determined by this technique are compiled in Fig. 3.

As expected, both 3DOM catalysts show a well-defined peak for pore radii around 40 nm. As it was shown in previous articles, the size of the PMMA spheres used as hard template are around 200 nm [28,29], that is, the PMMA spheres are larger than the pores created on the catalysts after removal of the template. This is mainly attributed to the reduction of the polymer volume during the thermal treatment. Note that the amount of pores with 40 nm radii increases for Cu/CeO<sub>2</sub>-3DOM with regard to CeO<sub>2</sub>-3DOM, which supports the hypothesis about the presence of closed porosity on CeO<sub>2</sub>-3DOM that is open after copper loading.

On the contrary, the reference samples prepared without template do not show this well-defined macroporosity in the pore size distributions of Fig. 3. The catalyst CeO<sub>2</sub>-Ref shows an increasing profile without relevant peaks, and Cu/CeO<sub>2</sub>-Ref shows a well-defined peak with maximum at 700 nm. These types of distributions are typical of solids where the main macroporosity comes from the interparticles space.

### 3.2. Catalysts characterization by XRD and Raman spectroscopy

The crystalline structure of the catalysts was characterized by XRD and Raman spectroscopy. Fig. 4 shows the X-Ray diffractograms of the catalysts, and Table 1 compiles several parameters determined from these diffractograms.

All diffractograms show the peaks of CeO<sub>2</sub>, with the main reflections typical of a fluorite-structured cubic material with fcc unit cell. The main peaks at 28.5, 33.1, 47.6, and 56.5° belong to the (111), (200), (220) and (311) planes [30], respectively, and are identified together with other lower-intensity peaks also attributed to the fluorite ceria lattice. The characteristic peaks of CuO are expected to appear at 35.5° and 38.8°, but they are not observed in Fig. 4, suggesting that copper species are either well dispersed on the ceria surface and/or copper cations are inserted into the ceria lattice.

The lattice constant of the fluorite phase was calculated for all catalysts, and the values are compiled in Table 1. Note that the lattice parameters are equal for 3DOM and Ref materials, suggesting that utilization of the PMMA template does not affect the primary crystals of ceria. The lattice parameters of the CeO<sub>2</sub>-3DOM and CeO<sub>2</sub>-Ref catalysts

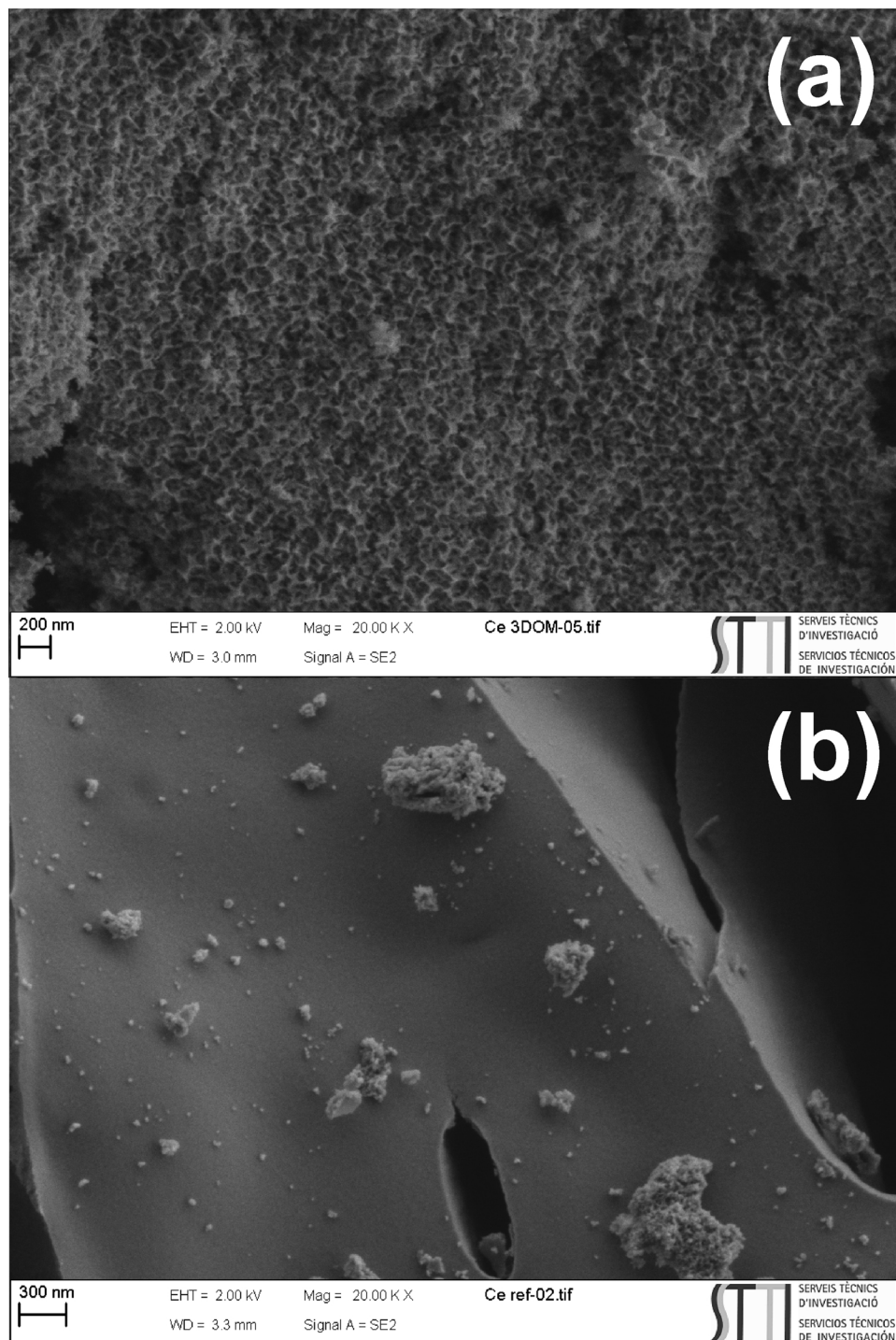


**Fig. 1.** FESEM images of the (a)  $\text{CeO}_2$ -3DOM and (b)  $\text{CeO}_2$ -Ref catalysts.

(0.5420 nm) are consistent with the value reported in the JCPDS 00-034-0394 reference database for this material, and the value of the pure ceria samples slightly decreased upon copper loading (0.5415 nm for Cu/ $\text{CeO}_2$ -3DOM and Cu/ $\text{CeO}_2$ -Ref). This could be attributed to the insertion of few copper cations into the ceria lattice. The Kim's equation was used to estimate the amount of copper inserted into the ceria lattice, and the results predict that 0.5% Cu is doping ceria (data in Table 1) for both copper containing catalysts (Cu/ $\text{CeO}_2$ -3DOM and Cu/ $\text{CeO}_2$ -Ref) while the remaining 1.5% is expected to be forming well dispersed segregated particles.

The crystallite sizes of the ceria fluorite phase are quite similar for

the four catalysts (21–28 nm), and this is an additional evidence supporting that the PMMA template does not affect the primary crystals of ceria. Minor differences are observed between values obtained with the Scherrer's and Williamson Hall's equations, suggesting that, in this case, crystal strain has a minor contribution to XRD peaks broadening.

Raman spectra were recorded for the four catalysts, and are shown in Fig. 5. The main band at  $465.5\text{ cm}^{-1}$  has been attributed to oxide anions vibration around their equilibrium positions in the octahedral sites of the fluorite lattice of ceria [31]. The position of this band is slightly higher for bare ceria samples than for copper-containing catalysts, because insertion of foreign copper cations affects the vibration of

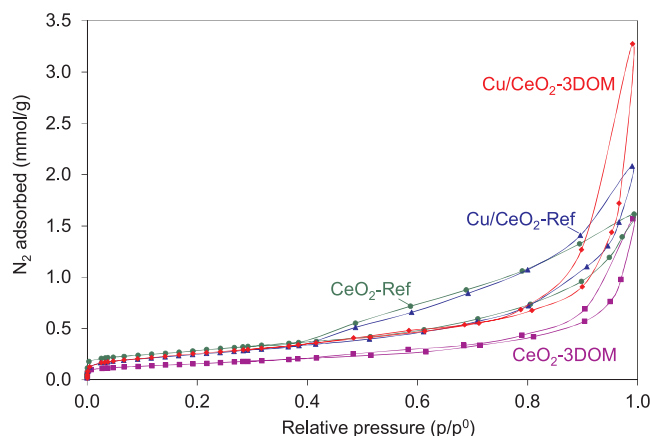


Fig. 2.  $\text{N}_2$  adsorption-desorption isotherms at  $-196^\circ\text{C}$  of the catalysts.

the oxide anions. However,  $\text{Cu}^{2+}$  cations are smaller than  $\text{Ce}^{4+}$  cations, and therefore, the shift of the  $\text{F}_{2g}$  band is expected to occur towards higher Raman Shift values, that is, the opposite trend observed in Fig. 5. This unexpected shift could be due to the partial reduction of  $\text{Ce}^{4+}$  to  $\text{Ce}^{3+}$  ( $\text{Ce}^{3+}$  being larger than  $\text{Ce}^{4+}$ ) to compensate the lattice contraction due to  $\text{Cu}^{2+}$  insertion. This argument is consistent with the creation of oxygen vacancies on ceria upon  $\text{Cu}^{2+}$  doping, as observed in Fig. 5b (see vacants band at  $595\text{ cm}^{-1}$ ), that is, the creation of oxygen vacancies could be due both to insertion of  $\text{Cu}^{2+}$  and to partial reduction of  $\text{Ce}^{4+}$  to  $\text{Ce}^{3+}$ . Fig. 5b also shows a band at  $1175\text{ cm}^{-1}$  attributed to surface oxygen species, probably superoxides [32], but differences among catalysts are minor.

### 3.3. Catalysts characterization by H<sub>2</sub>-TPR and XPS

The reducibility of the catalysts was studied by H<sub>2</sub>-TPR experiments, which were performed in a TG-MS set-up. Fig. 6 shows the  $m/z$  18 signal profiles, which belongs to  $\text{H}_2\text{O}$ . The band around  $100^\circ\text{C}$  is attributed to the release of adsorbed  $\text{H}_2\text{O}$ , and the bands at higher temperatures to  $\text{H}_2\text{O}$  yielded in  $\text{H}_2$  oxidation events. The highest-temperature bands around  $860^\circ\text{C}$  appear due to the reduction of  $\text{Ce}^{4+}$  cations located into the bulk ceria to  $\text{Ce}^{3+}$ , and these bands are qualitatively similar for the four catalysts.

The reduction of  $\text{Ce}^{4+}$  cations in the ceria surface takes place around  $500^\circ\text{C}$ , and this band is only observed for the 3DOM catalysts. Note that the surface area of the four samples is quite similar (see Table 1), and therefore, it must be concluded that the surface of the 3DOM samples is reduced more easily than that of the Ref samples. This feature of the 3DOM ceria samples was previously observed for Pr-doped ceria [28], and the improved reducibility resulted in a better catalytic activity for CO oxidation.

The copper-containing samples additionally show several  $\text{H}_2\text{O}$  peaks in the  $150$ – $280^\circ\text{C}$  range. The release of  $\text{H}_2\text{O}$  below  $200^\circ\text{C}$  is attributed to the reduction of copper oxide, and the release between  $200$  and  $280^\circ\text{C}$  to the copper-catalyzed surface ceria reduction, that is, to the reduction of surface  $\text{Ce}^{4+}$  cations that are in close contact with copper species. A rough estimation of the amounts of  $\text{H}_2$  consumed between  $150$  and  $280^\circ\text{C}$  confirms that not only  $\text{CuO}$  is reduced, but also part of the surface ceria.

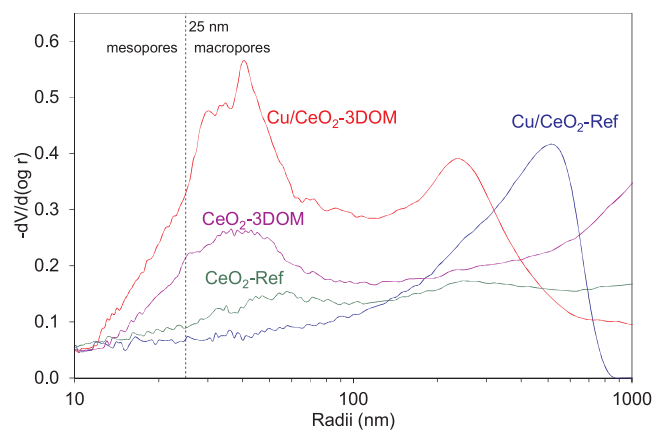


Fig. 3. Pore size distributions determined by mercury intrusion porosimetry.

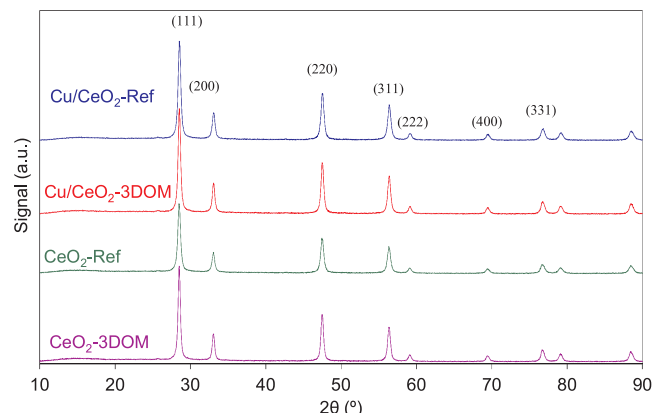


Fig. 4. X-Ray diffractograms of the catalysts.

Note that the reduction of copper cations in the Cu/CeO<sub>2</sub>-3DOM catalyst takes place in two steps (peaks at  $180$  and  $192^\circ\text{C}$ ) due to the presence of two different types of cationic species of copper with different reducibility. On the contrary, only one small copper oxide reduction peak (at  $182^\circ\text{C}$ ) appears in the Cu/CeO<sub>2</sub>-Ref catalyst. This suggests that the 3DOM structure affects the copper oxide-cerium oxide interaction. The copper oxide-cerium oxide interaction in the Cu/CeO<sub>2</sub>-3DOM catalyst seems to be poor, because copper cations are first reduced and the copper-catalyzed ceria reduction takes place afterwards. This poor interaction is attributed to the difficult penetration of the  $\text{Cu}^{2+}$  impregnation solution into the 3DOM structure. On the contrary, the copper oxide-cerium oxide interaction seems to be much better on Cu/CeO<sub>2</sub>-Ref, because the two typical CuO reduction peaks are not observed, and instead, a main peak at  $235^\circ\text{C}$  appears, which can be attributed to the reduction of the copper oxide-cerium oxide interface.

XPS was used to analyze the surface of the catalysts and Fig. 7a shows the Cu 2p region in terms of binding energy. The Cu 2p3/2 region shows a broad band with two contributions with peak maxima at  $934.2$  and  $932.4\text{ eV}$ . These values can be assigned to copper oxidized species with different electronic environment, while the presence of the

Table 1

Results of the catalysts characterization by  $\text{N}_2$  adsorption, He density, XRF and XRD.

Catalyst	BET ( $\text{m}^2/\text{g}$ )	He density ( $\text{g}/\text{cm}^3$ )	Total Cu by XRF (%)	Cu doped into $\text{CeO}_2$ lattice (%)	Fluorite Lattice constant (nm)	Fluorite crystallite size Scherrer (nm)	Fluorite crystallite size W-H (nm)
Cu/CeO <sub>2</sub> -Ref	21	7.1	$1.7 \pm 0.1$	0.5	0.5415	23	24
Cu/CeO <sub>2</sub> -3DOM	21	7.2	$2.2 \pm 0.2$	0.5	0.5415	25	24
CeO <sub>2</sub> -Ref	23	6.9	–	–	0.5420	21	28
CeO <sub>2</sub> -3DOM	12	6.9	–	–	0.5420	26	27

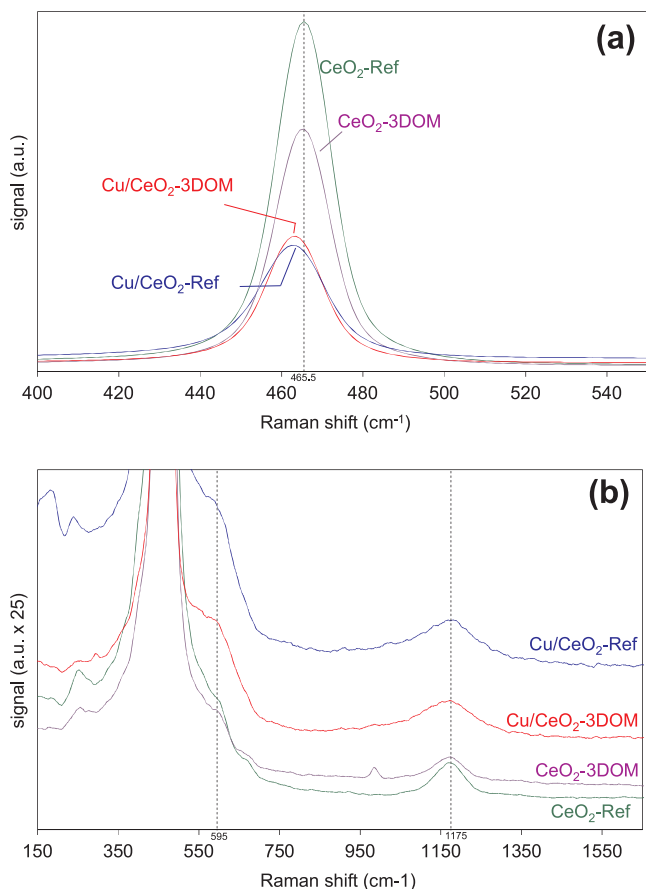


**Fig. 5.** Raman spectra of the catalysts. (a) Detail of the F<sub>2g</sub> band and (b) detail of the vacants and surface oxygen bands. Y-axis scale is 25 times magnified in (b) with regard to (a).

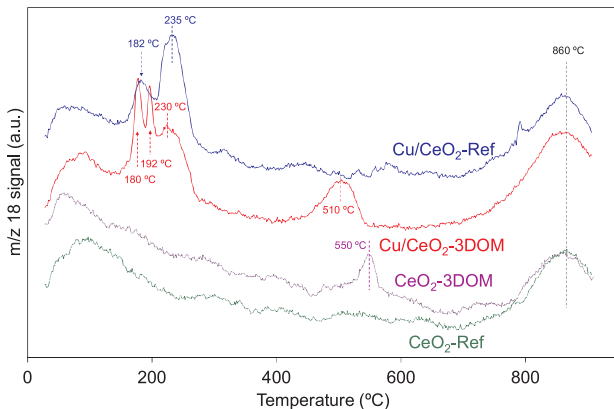


**Fig. 6.** H<sub>2</sub>-TPR characterization of the catalysts.

shake-up satellite peaks confirms the presence of Cu<sup>2+</sup> cations [33,34].

On the other hand, the Cu L<sub>3</sub>M<sub>4.5</sub>M<sub>4.5</sub> Auger line (Fig. 7b) shows one main peak centered at 916.7 eV, which is tentatively ascribed to the lone presence of Cu<sup>2+</sup> species [35]. Therefore, the two cationic species identified in Cu 2p3/2 spectra must correspond to Cu<sup>2+</sup> in different interaction with CeO<sub>2</sub> support. When comparing both catalysts, the contribution with lower binding energy is more intense for Cu/CeO<sub>2</sub>-Ref, which evidences higher interaction of CuO-CeO<sub>2</sub> phases by promotion of Cu<sup>2+</sup> partial reduction. The composition of the catalysts surface was determined by XPS and the results are compiled in Table 2 together with the percentage of Ce<sup>3+</sup> cations with regard to total Ce<sup>3+</sup> + Ce<sup>4+</sup>. The Ce 3d spectra are included in the supplementary material,

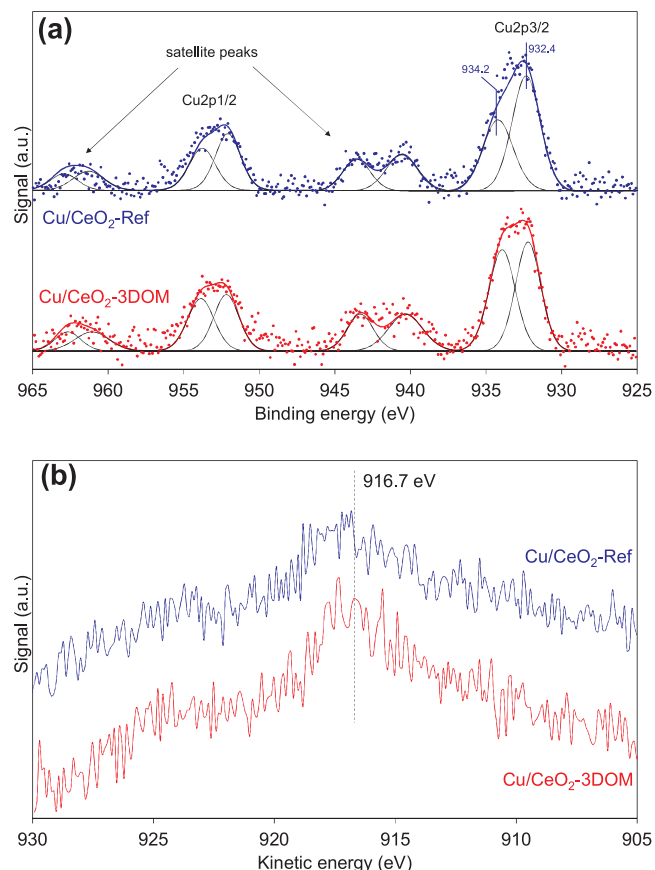


**Fig. 7.** XPS characterization of the catalysts surface. (a) Cu 2p photoemission region and (b) Cu L<sub>3</sub>M<sub>4.5</sub>M<sub>4.5</sub> Auger transition range.

**Table 2**  
Surface characterization by XPS.

Catalyst	C (%)	O (%)	Ce (%)	Cu (%)	Ce <sup>+3</sup> (%)
Cu/CeO <sub>2</sub> -Ref	30.9	47.9	16.9	4.3	36
Cu/CeO <sub>2</sub> -3DOM	30.3	49.3	17.1	3.3	40
CeO <sub>2</sub> -Ref	41.3	41.8	16.9	–	35
CeO <sub>2</sub> -3DOM	51.1	38.2	10.7	–	35

and the Ce<sup>3+</sup> percentages were calculated after deconvolution of the spectra, dividing the ratio of the sum of areas of the u<sub>0</sub>, u<sub>1</sub>, v<sub>0</sub>, and v<sub>1</sub> bands between to the sum of the areas of all bands [36].

The Ce<sup>3+</sup> percentage is similar for all catalysts (35–40 %), and the most relevant differences are noticed in the carbon concentration. It was concluded from porosity characterization that part of the porosity of the CeO<sub>2</sub>-3DOM catalyst is closed due to carbonates blocking, and the high concentration of surface carbon on this catalyst (51.1%) is consistent with this hypothesis. It was also concluded that this closed porosity is open after copper impregnation, because the slightly acid pH of the copper solution used for impregnation destabilizes carbonates, which are evolved. This hypothesis is also consistent with the lower surface carbon concentration on the Cu/CeO<sub>2</sub>-3DOM catalyst (30.3%) with regard to that on CeO<sub>2</sub>-3DOM. Note that the decrease of the surface carbon concentration after copper impregnation is also observed in the reference samples, but in a lower extent.

As a summary, the main conclusion of the catalysts characterization, for the purposes of this study, is that the 3DOM structure has been properly obtained, and clear differences in the porosity have been observed with regard to the reference samples. The primary ceria crystals are quite similar for the four catalysts, and the CuO-Ceria interaction is much better on Cu/CeO<sub>2</sub>-Ref than on Cu/CeO<sub>2</sub>-3DOM.

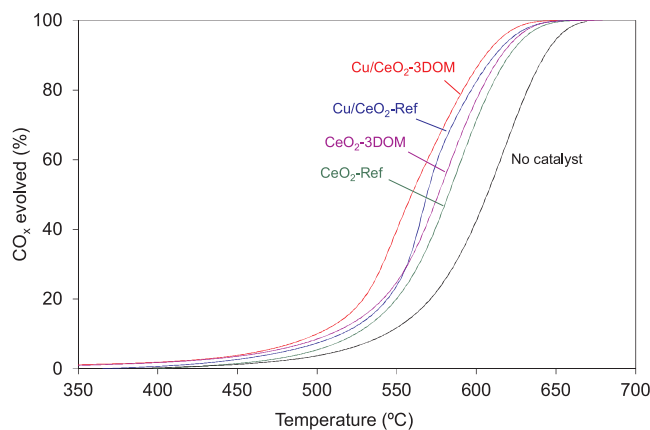


Fig. 8. Soot combustion experiments with 5% O<sub>2</sub> + N<sub>2</sub>.

### 3.4. Catalytic combustion of soot with O<sub>2</sub>

Soot combustion experiments were performed under 5%O<sub>2</sub>/N<sub>2</sub>, and the CO<sub>x</sub> evolution profiles are shown in Fig. 8. The percentage of CO evolved with regard to total CO<sub>x</sub> is included in Table 3.

All catalysts accelerate the combustion of soot with regard to the uncatalyzed reaction. The uncatalyzed reaction yields more CO (59.8%) than CO<sub>2</sub>, while CO<sub>2</sub> is the main soot combustion product of the catalytic reactions. The copper-containing catalysts reach the CO<sub>2</sub> selectivity until values near 100%.

The catalytic activity depends both on the catalyst composition and morphology. CeO<sub>2</sub>-Ref is the least active catalyst, and the 3DOM structure (CeO<sub>2</sub>-3DOM catalyst) improves the catalytic activity for soot combustion. Copper additionally accelerates the combustion with O<sub>2</sub>, Cu/CeO<sub>2</sub>-3DOM being the most active catalyst. According to these results, the catalytic activity for soot combustion in 5%O<sub>2</sub>/N<sub>2</sub> follows the trend Cu/CeO<sub>2</sub>-3DOM > Cu/CeO<sub>2</sub>-Ref > CeO<sub>2</sub>-3DOM > CeO<sub>2</sub>-Ref.

The ceria-catalyzed combustion of soot with O<sub>2</sub> takes place by the so-called active oxygen mechanism [4,11]. In this mechanism, the combustion of soot takes place with catalyst oxygen, partially reducing Ce<sup>4+</sup> cations to Ce<sup>3+</sup>, and the oxygen vacancies created on the catalyst are filled with gas phase molecular O<sub>2</sub>. This mechanism has two critical steps, being the production of active oxygen and the transfer of active oxygen from catalyst to soot particles. In the one hand, the production of active oxygen depends on the physical-chemical properties of the ceria catalyst, and the introduction of dopants affects significantly the amount of active oxygen available in a ceria-based catalyst [6,15,17,18]. On the other hand, it is postulated that active oxygen species are oxygen radicals with short lifetime [12], and their transfer from the solid catalyst to soot particles is restricted to the limited contact points available. It has been postulated that the macroporous 3DOM structures improve the soot-catalyst contact [21,22], and this would explain the improved catalytic activity observed in Fig. 8 for the 3DOM catalysts.

In order to get insight into the role of the production and transfer of active oxygen for the catalysts evaluated in this study, oxygen exchange

experiments were performed at 450 °C with isotopic O<sub>2</sub>. Fig. 9 shows the gas profiles monitored during pulses of Ar and <sup>18</sup>O<sub>2</sub> to the catalysts.

The Ar profiles are used as a reference to monitor the diffusion of an inert gas throughout the catalytic beds. After the interaction of <sup>18</sup>O<sub>2</sub> with the catalysts, three oxygen species were detected, <sup>18</sup>O<sub>2</sub>, <sup>16</sup>O<sub>2</sub> and <sup>18</sup>O<sup>16</sup>O, where <sup>18</sup>O comes from the molecular oxygen pulsed and <sup>16</sup>O comes from the catalyst. Total O<sub>2</sub> profiles were calculated as the sum of the three O<sub>2</sub> contributions, and for all catalysts, the total O<sub>2</sub> profile overlaps the reference Ar profile. This means that the time required for the oxygen exchange steps to occur is negligible in comparison to the time required for gases to diffuse through the catalytic bed. Previous oxygen exchange experiments performed in a TAP reactor showed that the oxygen exchange takes place in a time frame below the milliseconds [1].

Quantification of the area under the different O<sub>2</sub> species provides valuable information about the catalytic combustion of soot by active oxygen. The amount of <sup>18</sup>O<sub>2</sub> detected after the pulse to CeO<sub>2</sub>-3DOM (Fig. 9c; 60% of the total area of the sum of all O<sub>2</sub> species) is slightly lower to that detected for CeO<sub>2</sub>-Ref (Fig. 9d; 66%), that is, the 3DOM structure improves the exchange of oxygen and the production of active oxygen. In addition, CeO<sub>2</sub>-3DOM favors the double exchange of oxygen atoms (26% <sup>16</sup>O<sub>2</sub> vs 14% <sup>18</sup>O<sup>16</sup>O) while in the reference ceria prevail the scramble molecules (15% <sup>16</sup>O<sub>2</sub> vs 19% <sup>18</sup>O<sup>16</sup>O). Therefore, it can be concluded that the improved catalytic activity for soot combustion of CeO<sub>2</sub>-3DOM with regard to CeO<sub>2</sub>-Ref must be not only attributed to the improved soot-catalyst contact, but also to the higher production of active oxygen. A similar conclusion was achieved for the 3DOM ceria-catalyzed oxidation of CO [28], where it was proposed that the O<sub>2</sub>-poor environment created into the macroporous structure of the 3DOM ceria during the combustion of the PMMA template and decomposition/oxidation of citrates leads of the formation of a more reactive ceria surface with improved redox properties.

The effect of copper in the exchange of oxygen depends on the type of ceria considered. The exchange of oxygen by Cu/CeO<sub>2</sub>-Ref (Fig. 9b) is significantly improved with regard to CeO<sub>2</sub>-Ref (Fig. 9d), but this improvement is not so obvious in Cu/CeO<sub>2</sub>-3DOM (Fig. 9a) with regard to CeO<sub>2</sub>-3DOM (Fig. 9c). These differences must be attributed to differences in the CuO-CeO<sub>2</sub> contact. As deduced from H<sub>2</sub>-TPR characterization (Fig. 6) CuO-CeO<sub>2</sub> contact is better on Cu/CeO<sub>2</sub>-Ref than on Cu/CeO<sub>2</sub>-3DOM, and the oxygen exchange experiments evidence that this better contact is very positive to improve exchange of oxygen. It is reasonable to think that the improved surface reducibility of the Cu/CeO<sub>2</sub>-Ref catalyst upon copper loading favors the redox steps taking place during the exchange process. The improved exchange of oxygen would explain the improved catalytic activity for soot combustion of Cu/CeO<sub>2</sub>-Ref with regard to CeO<sub>2</sub>-Ref (Fig. 8), since more active oxygen is created by the copper-containing catalyst.

On the contrary, copper has almost no effect in the exchange of oxygen by Cu/CeO<sub>2</sub>-3DOM (Fig. 9a) with regard to CeO<sub>2</sub>-3DOM (Fig. 9c) due to the poor copper oxide-cerium oxide contact. In this case, the improved catalytic activity for soot combustion of the copper-containing catalyst (Fig. 8) must be attributed to the higher macroporosity available (Fig. 4) because the acid pH of the Cu<sup>2+</sup> impregnation solution removes carbonates opening closed porosity.

The different effect of copper on the 3DOM and Ref cerias is also observed comparing Fig. 9a and b, where considerably lower percentage of <sup>18</sup>O<sub>2</sub> and higher <sup>16</sup>O<sub>2</sub> is observed for Cu/CeO<sub>2</sub>-3DOM (Fig. 9a). This indicates that active oxygen generation in Cu/CeO<sub>2</sub>-3DOM is worse than in Cu/CeO<sub>2</sub>-Ref (Fig. 9b). This confirms that the formation of the 3DOM structure is showing a negative influence on the Cu containing catalyst. As deduced from H<sub>2</sub>-TPR, there should exist a well-defined Cu-O-Ce interface in the Cu/CeO<sub>2</sub>-Ref catalyst while not on Cu/CeO<sub>2</sub>-3DOM, and the loosely bound interfacial oxygen atoms probably lead to the generation of higher amount of active oxygen.

In conclusion, these experiments confirm that the two critical steps in the ceria-catalyzed soot combustion by O<sub>2</sub> are the creation of active

Table 3  
CO evolved with regard to total CO<sub>x</sub> (=CO + CO<sub>2</sub>) in soot combustion experiments.

Catalyst	Experiments with 5% O <sub>2</sub> + N <sub>2</sub>	Experiments with 500 ppm NO <sub>x</sub> + 5% O <sub>2</sub> + N <sub>2</sub>
Cu/CeO <sub>2</sub> -Ref	1.5	0.7
Cu/CeO <sub>2</sub> -3DOM	4.2	6.5
CeO <sub>2</sub> -Ref	16.6	34.5
CeO <sub>2</sub> -3DOM	29.0	46.0
No catalyst	59.8	63.7

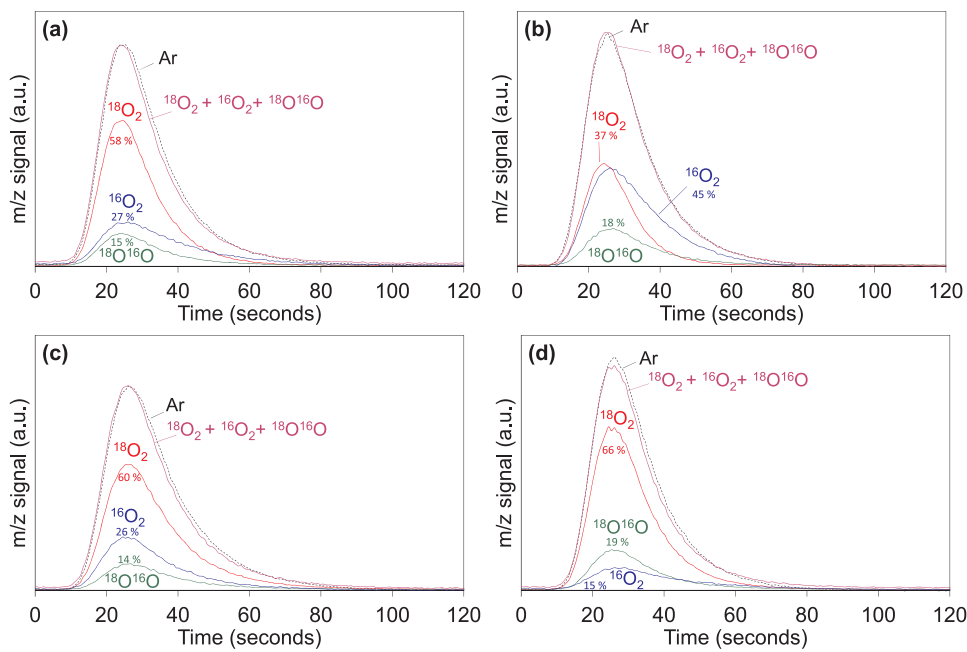


**Fig. 9.** O<sub>2</sub> and Ar profiles in oxygen exchange experiments at 450 °C. (a) Cu/CeO<sub>2</sub>-3DOM, (b) Cu/CeO<sub>2</sub>-Ref, (c) CeO<sub>2</sub>-3DOM y (d) CeO<sub>2</sub>-Ref.

oxygen by the ceria catalyst and the transfer of active oxygen from catalyst to soot. The 3DOM structure improves both the creation of active oxygen and the transfer of such oxygen to soot, and the role of copper depends significantly on the copper oxide-cerium oxide contact. If contact is good the creation of active oxygen is improved, but not if the contact is poor.

### 3.5. Catalytic combustion of soot with NO<sub>x</sub> + O<sub>2</sub>

The effect of NO<sub>x</sub> in the catalytic combustion of soot was studied, and two type of experiments were performed using a gas mixture with NO<sub>x</sub> + O<sub>2</sub>. The catalytic combustion of soot was studied with soot + catalyst mixtures and the catalytic oxidation of NO to NO<sub>2</sub> was studied in experiments performed only with the catalysts (without soot).

Fig. 10 shows the CO<sub>x</sub> evolution profiles in soot combustion experiments performed with NO<sub>x</sub> + O<sub>2</sub>, where it is observed that all catalysts accelerate the combustion of soot with regard to the uncatalyzed reaction. The CO selectivity values were included in Table 3, and the uncatalyzed reaction yields more CO (63.7%) than CO<sub>2</sub>. In agreement with the experiments performed without NO<sub>x</sub> in the gas mixture, CO<sub>2</sub> is the main soot combustion product of the catalytic

reactions, and the copper-containing catalysts reach very high CO<sub>2</sub> selectivity values.

In accordance with the experiments performed in the absence of NO<sub>x</sub> (Fig. 8), CeO<sub>2</sub>-Ref also shows the lowest activity to accelerate soot combustion in the presence of NO<sub>x</sub> (Fig. 10). Both the 3DOM structure and the incorporation of copper improve the catalytic activity, but the trends observed in the absence (Fig. 8) and presence (Fig. 10) of NO<sub>x</sub> are different, because the reaction mechanisms are also different. The ceria-catalyzed combustion of soot with O<sub>2</sub>, as mentioned, is based on the formation and transfer of active oxygen from catalyst to soot. In the presence of NO<sub>x</sub>, additionally, NO<sub>2</sub> also participates as it is an efficient soot oxidizing gas that is formed by catalytic oxidation of NO. In the presence of NO<sub>x</sub>, the NO<sub>2</sub>-assisted combustion of soot takes place together with the active oxygen mechanism.

The catalytic combustion of soot in the absence and presence of NO<sub>x</sub> has been compared using the temperature for 50% soot combustion (T50%), and the T50% values are compiled in Fig. 11.

NO<sub>x</sub> has a minor effect in the direct combustion of soot (without catalyst) and the T50% temperature is slightly higher in the presence of NO<sub>x</sub>. This small inhibition of the soot reactivity in the presence of NO<sub>x</sub> can be attributed to the chemisorption of NO<sub>x</sub> on the carbon surface [37,38], which blocks unsaturated carbon sites during the combustion

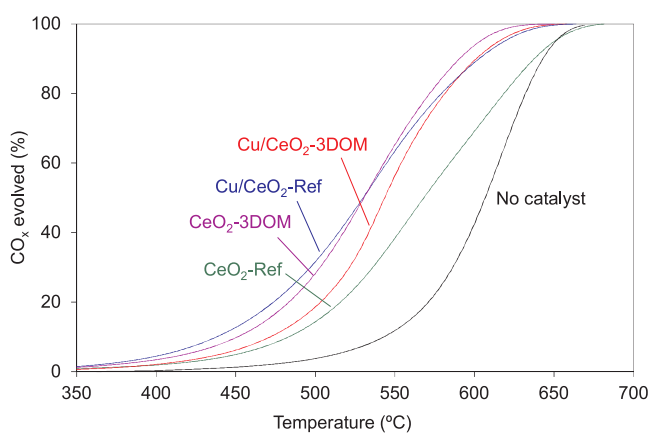


**Fig. 10.** Soot combustion experiments with 500 ppm NO<sub>x</sub> + 5% O<sub>2</sub> + N<sub>2</sub>.

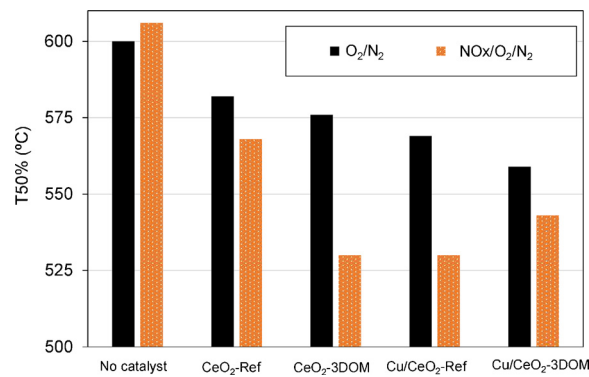


**Fig. 11.** Temperature for 50% soot combustion in experiments performed with and without NO<sub>x</sub> in the gas mixture.

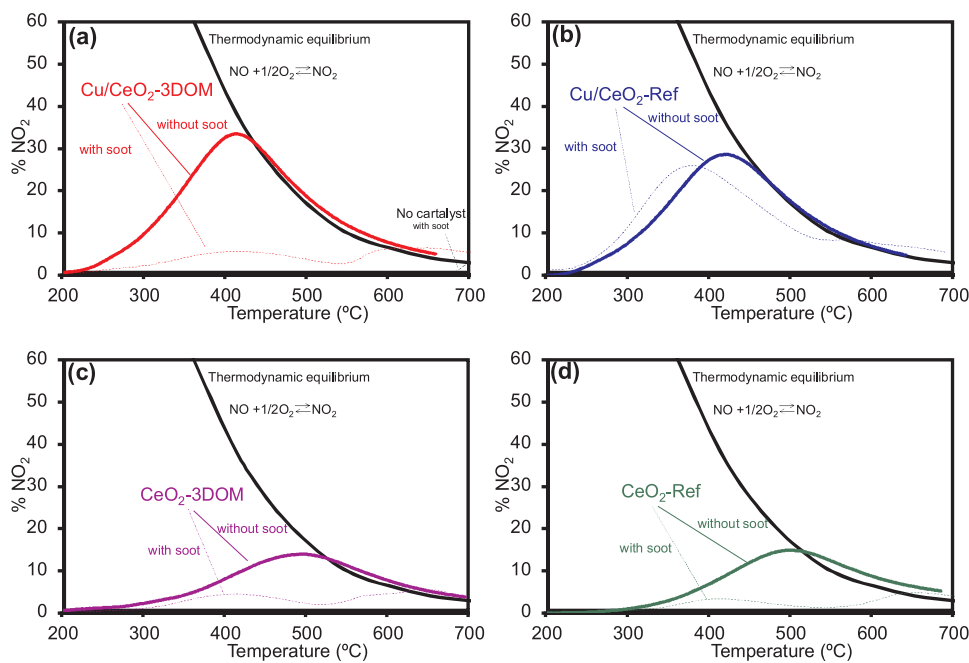


**Fig. 12.** NO<sub>2</sub> profiles in catalytic experiments performed with and without soot. (a) Cu/CeO<sub>2</sub>-3DOM, (b) Cu/CeO<sub>2</sub>-Ref, (c) CeO<sub>2</sub>-3DOM and (d) CeO<sub>2</sub>-Ref.

and hinders further chemisorption of O<sub>2</sub>, which is the main oxidizing molecule in this case.

NOx decreases the T50% temperature for all catalysts, but the effect is much more relevant for CeO<sub>2</sub>-3DOM and Cu/CeO<sub>2</sub>-Ref than for CeO<sub>2</sub>-Ref and Cu/CeO<sub>2</sub>-3DOM. These differences can be explained analyzing the NO<sub>2</sub> (Fig. 12) profiles during the catalytic experiments performed with and without soot.

NO is the main nitrogen oxide in the gas stream feed to the reactor, and all catalysts accelerate the oxidation to NO<sub>2</sub>. In the absence of soot, the NO<sub>2</sub> profiles increase with temperature until a maximum where thermodynamic equilibrium is achieved, and above that temperature the NO<sub>2</sub> profiles decrease following thermodynamics (Fig. 12).

The catalytic activity for NO oxidation to NO<sub>2</sub> is higher for the copper-containing catalysts than for the pure ceria samples, which was something expected [39], and the 3DOM structure has a minor effect in NO<sub>2</sub> formation. The NO<sub>2</sub> produced by the catalysts reacts with soot during the soot combustion experiments, as deduced comparing the NO<sub>2</sub> profiles obtained with and without soot. Most NO<sub>2</sub> produced by Cu/CeO<sub>2</sub>-3DOM, CeO<sub>2</sub>-3DOM and CeO<sub>2</sub>-Ref (Fig. 12a, c and d, respectively) is consumed by reaction with soot, but this is not obvious for Cu/CeO<sub>2</sub>-Ref (Fig. 12b). The anomalous behavior of Cu/CeO<sub>2</sub>-Ref could be explained in two different ways. It could be argued that the NO<sub>2</sub> produced is not reacting with soot in this case, or that each NO molecule is oxidized several times during the residence time into the catalytic bed, that is, NO is oxidized to NO<sub>2</sub> and NO<sub>2</sub> is reduced to NO by soot afterwards. The second argument seems more reasonable in this case, and the high NO<sub>2</sub> level detected in the presence of soot would mean that the catalytic oxidation rate of NO to NO<sub>2</sub> is much faster than the NO<sub>2</sub> reduction rate by soot.

It is known that NO is the main nitrogen-containing product of the NO<sub>2</sub>-soot reaction [13], but it has been also reported that the NOx-soot reaction also yields some N<sub>2</sub> [40]. This is deduced from the NOx profiles included in Fig. 13.

There are not evidences of net NOx removal from the gas stream in the 200–700 °C range during the catalytic experiments performed without soot. On the contrary, all NOx profiles obtained in experiments performed with soot show a minimum that must be attributed to NOx reduction by soot, which occurs together with soot gasification.

Finally, the effect of the 3DOM structure and copper in the soot

combustion mechanism using ceria catalysts and NOx + O<sub>2</sub> mixtures can be discussed. As a general behavior, NOx always improves the combustion of soot with regard to O<sub>2</sub> combustion because all catalysts accelerate NO to NO<sub>2</sub>, and NO<sub>2</sub> is a powerful soot oxidant. This seems to be the main soot combustion mechanism for "Ref" samples. CeO<sub>2</sub>-Ref is the least active catalyst for O<sub>2</sub> combustion, because it has poor capacity for active oxygen production and transfer to soot. In the presence of NOx, the CeO<sub>2</sub>-Ref-catalysed oxidation rate increases because few NO<sub>2</sub> is produced and the NO<sub>2</sub>-assisted mechanism participates in a certain extent. Incorporation of copper to CeO<sub>2</sub>-Ref (Cu/CeO<sub>2</sub>-Ref catalyst) improves the production of active oxygen, but not the transfer of active oxygen to soot, and that is why the catalytic activity for soot combustion with O<sub>2</sub> only increases slightly for Cu/CeO<sub>2</sub>-Ref with regard to CeO<sub>2</sub>-Ref. However, Cu/CeO<sub>2</sub>-Ref is very efficient for soot combustion in the presence of NOx because NO<sub>2</sub> has not restrictions to travel from catalyst to soot. Copper also improves the catalytic oxidation of NO to NO<sub>2</sub> (Cu/CeO<sub>2</sub>-Ref) with regard to pure ceria (CeO<sub>2</sub>-Ref) and NO<sub>2</sub> can oxidize soot efficiently.

The role of the 3DOM structure in the soot combustion mechanism is much more complex. In the O<sub>2</sub> combustion, the 3DOM structure (CeO<sub>2</sub>-3DOM catalyst) improves the production and transfer of active oxygen from catalyst to soot with regard to the conventional structure (CeO<sub>2</sub>-Ref). The catalytic combustion of soot using CeO<sub>2</sub>-3DOM is accelerated very efficiently in the presence of NOx, in spite of the production NO<sub>2</sub> is not very high (see Fig. 12). This must be attributed to the contribution of NO<sub>2</sub> to the active oxygen mechanism. It has been reported [11] that NO<sub>2</sub>, once produced by a ceria catalyst, can either travel in the gas phase and react with soot or be re-adsorbed on the ceria surface yielding chemisorbed NO and active oxygen, that is, NO<sub>2</sub> is an efficient way not only for direct soot oxidation but also for active oxygen production. In ceria catalysts with a conventional structure, the main role of NO<sub>2</sub> in the catalytic combustion of soot is the direct oxidation of soot by NO<sub>2</sub>, because active oxygen has restrictions to be transferred from catalyst to soot. However, the 3DOM structure improves the transfer of active oxygen, and therefore, an additional benefit is obtained from NO<sub>2</sub>, that is, NO<sub>2</sub> contributes to active oxygen production and the 3DOM structure allows the efficient transfer to soot. This efficient utilization of active oxygen by CeO<sub>2</sub>-3DOM explains why soot combustion in the presence of NOx occurs as fast as with Cu/CeO<sub>2</sub>-

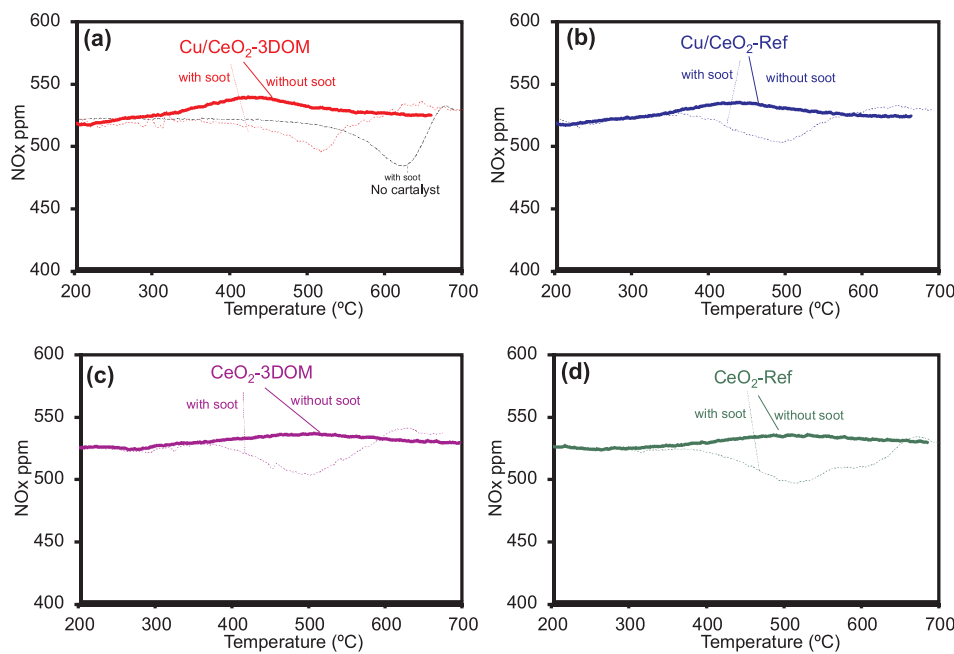


**Fig. 13.** NO<sub>x</sub> profiles in catalytic experiments performed with and without soot. (a) Cu/CeO<sub>2</sub>-3DOM, (b) Cu/CeO<sub>2</sub>-Ref, (c) CeO<sub>2</sub>-3DOM and (d) CeO<sub>2</sub>-Ref.

Ref, which accelerates combustion mainly by direct NO<sub>2</sub> oxidation.

This benefit is not observed for Cu/CeO<sub>2</sub>-3DOM because the CuO-CeO<sub>2</sub> contact is poor. In this case, copper improves the catalytic oxidation of NO to NO<sub>2</sub> with regard to CeO<sub>2</sub>-3DOM (compare Fig. 12a and c), and NO<sub>2</sub> oxidizes soot but not contributes to active oxygen production. This explains the moderate improvement in soot combustion using Cu/CeO<sub>2</sub>-3DOM in the presence of NO<sub>x</sub> with regard to O<sub>2</sub> combustion, because NO<sub>2</sub> only reacts with soot but not produces additional active oxygen. The faster oxidation of soot using Cu/CeO<sub>2</sub>-Ref with regard to Cu/CeO<sub>2</sub>-3DOM can be attributed to the better CuO-CeO<sub>2</sub> contact, which seems to affect the NO oxidation rate allowing a more efficient utilization of the NO molecules that are oxidized and reduced several times while they are inside the catalytic bed.

According to these results, future efforts must be focused on the preparation of a Cu/CeO<sub>2</sub>-3DOM soot combustion catalyst with good dispersion of copper to improve the CuO-CeO<sub>2</sub> contact, therefore obtaining the double benefit of high amount of active oxygen production due to NO<sub>2</sub> participation and efficient active oxygen transfer from catalyst to soot due to the 3DOM structure.

#### 4. Conclusions

The participation of the active oxygen and NO<sub>2</sub>-assisted soot combustion mechanisms has been studied for 3DOM ceria catalysts with and without copper, and the behavior has been compared with that of similar reference materials without 3DOM structure.

All ceria catalysts accelerate soot combustion with O<sub>2</sub>, which only occurs by the active oxygen mechanism, and both the 3DOM structure and the presence of copper improve the activity. The CeO<sub>2</sub>-3DOM catalyst produces more active oxygen than the reference counterpart catalyst CeO<sub>2</sub>-Ref, and this active oxygen is transferred more efficiently to soot due to the macroporous structure. Copper improves the exchange of oxygen between ceria and O<sub>2</sub>, therefore improving the production of active oxygen, but this improvement is only observed if the CuO-CeO<sub>2</sub> contact is good. An appropriate CuO-CeO<sub>2</sub> contact is achieved by impregnation of the conventional CeO<sub>2</sub>-Ref support but not for CeO<sub>2</sub>-3DOM due to the difficult diffusion of the impregnation solution into the macroporous network.

In the presence of NO<sub>x</sub> + O<sub>2</sub>, all ceria catalysts prepared and tested accelerate NO oxidation to NO<sub>2</sub>, and NO<sub>2</sub> is a powerful soot oxidant

that accelerates soot combustion with regard to the O<sub>2</sub>-only combustion. CeO<sub>2</sub>-3DOM and CeO<sub>2</sub>-Ref have the same activity for NO oxidation to NO<sub>2</sub>, but CeO<sub>2</sub>-3DOM utilizes NO<sub>2</sub> more efficiently than CeO<sub>2</sub>-Ref for soot combustion. This is because part of the NO<sub>2</sub> produced oxidizes soot and part is devoted to the further production of active oxygen, which is more oxidizing than NO<sub>2</sub>. In ceria catalysts with a conventional structure, the main role of NO<sub>2</sub> in the catalytic combustion of soot is the direct oxidation of soot by NO<sub>2</sub>, because active oxygen has restrictions to be transferred from catalyst to soot. However, the 3DOM structure improves the transfer of active oxygen, and therefore, an additional benefit is obtained from NO<sub>2</sub>, that is, NO<sub>2</sub> contributes to active oxygen production and the 3DOM structure allows its efficient transfer to soot.

#### Acknowledgements

The authors thank the financial support of Generalitat Valenciana (Project PROMETEOII/2014/010), the Spanish Ministry of Economy and Competitiveness (Project CTQ2015-67597-C2-2-R), the Spanish Ministry of Education, Culture and Sports (grant FPU14/01178) and the UE (FEDER funding).

#### Appendix A. Supplementary data

Supplementary data associated with this article can be found, in the online version, at <https://doi.org/10.1016/j.apcatb.2018.04.023>.

#### References

- [1] A. Bueno-López, K. Krishna, M. Makkee, J.A. Moulijn, Enhanced soot oxidation by lattice oxygen via La<sup>3+</sup>-doped CeO<sub>2</sub>, *J. Catal.* 230 (2005) 237–248.
- [2] E. Aneggi, M. Boaro, C. De Leitenburg, G. Dolcetti, A. Trovarelli, Insights into the redox properties of ceria-based oxides and their implications in catalysis, *J. Alloys Compd.* 408–412 (2006) 1096–1102.
- [3] E. Aneggi, C. de Leitenburg, G. Dolcetti, A. Trovarelli, Promotional effect of rare earths and transition metals in the combustion of diesel soot over CeO<sub>2</sub> and CeO<sub>2</sub>-ZrO<sub>2</sub>, *Catal. Today* 114 (2006) 40–47.
- [4] A. Bueno-López, Diesel soot combustion ceria catalysts, *Appl. Catal. B* 146 (2014) 1–11.
- [5] L. Katta, P. Sudarsanam, G. Thrimurthulu, B.M. Reddy, Doped nanosized ceria solid solutions for low temperature soot oxidation: Zirconium versus lanthanum promoters, *Appl. Catal. B* 101 (2010) 101–108.
- [6] M. Piumetti, S. Bensaid, N. Russo, D. Fino, Nanostructured ceria-based catalysts for soot combustion: investigations on the surface sensitivity, *Appl. Catal. B* 165 (2015)

- 742–751.
- [7] G. Kim, Ceria-promoted three-way catalysts for auto exhaust emission control, *Ind. Eng. Chem. Prod. Res. Dev.* 21 (1982) 267–274.
  - [8] A.F. Diwell, R.R. Rajaram, H.A. Shaw, T.J. Truex, The role of ceria in three-way catalysts, *Stud. Surf. Sci. Catal.* 71 (1991) 139–152.
  - [9] H.S. Gandhi, G.W. Graham, Mc Cabe. R.W, Automotive exhaust catalysis, *J. Catal.* 216 (2003) 433–442.
  - [10] N. Guillén-Hurtado, A. García-García, A. Bueno-López, Isotopic study of ceria-catalyzed soot oxidation in the presence of NO<sub>x</sub>, *J. Catal.* 299 (2013) 181–187.
  - [11] A. Setiabudi, J. Chen, G. Mul, M. Makkee, J.A. Moulijn, CeO<sub>2</sub> catalysed soot oxidation: the role of active oxygen to accelerate the oxidation conversion, *Appl. Catal. B* 51 (2004) 9–19.
  - [12] A. Bueno-López, K. Krishna, M. Makkee, J.A. Moulijn, Active oxygen from CeO<sub>2</sub> and its role in catalysed soot oxidation, *Catal. Lett.* 99 (2005) 203–205.
  - [13] A. Setiabudi, M. Makkee, J.A. Moulijn, The role of NO<sub>2</sub> and O<sub>2</sub> in the accelerated combustion of soot in diesel exhaust gases, *Appl. Catal. B* 50 (2004) 185–194.
  - [14] N. Guillén-Hurtado, A. García-García, A. Bueno-López, Active oxygen by Ce-Pr mixed oxide nanoparticles outperform diesel soot combustion Pt catalysts, *Appl. Catal. B* 174 (2015) 60–66.
  - [15] H. Huang, J. Liu, P. Sun, S. Ye, B. Liu, Effects of Mn-doped ceria oxygen-storage material on oxidation activity of diesel soot, *RSC Adv.* 7 (2017) 7406–7412.
  - [16] M. Piumetti, T. Andana, S. Bensaid, D. Fino, N. Russo, R. Pirone, Ceria-based nanomaterials as catalysts for CO oxidation and soot combustion: effect of Zr-Pr doping and structural properties on the catalytic activity, *AIChE J.* 63 (2017) 216–225.
  - [17] D. Mukherjee, B.G. Rao, B.M. Reddy, CO and soot oxidation activity of doped ceria: influence of dopants, *Appl. Catal. B* 197 (2016) 105–115.
  - [18] P. Dulgheru, J.A. Sullivan, Rare earth (La, Nd, Pr) doped ceria zirconia solid solutions for soot combustion, *Top. Catal.* 56 (2013) 504–510.
  - [19] A. Trovarelli, J. Llorca, Ceria catalysts at nanoscale: how do crystal shapes shape catalysis? *ACS Catal.* 7 (2017) 4716–4735.
  - [20] E. Aneggi, D. Wiater, C. De Leitenburg, J. Llorca, A. Trovarelli, Shape-dependent activity of ceria in soot combustion, *ACS Catal.* 4 (2014) 172–181.
  - [21] G. Zhang, Z. Zhao, J. Liu, G. Jiang, A. Duan, J. Zheng, S. Chen, R. Zhou, Three dimensionally ordered macroporous Ce<sub>1-x</sub>Zr<sub>x</sub>O<sub>2</sub> solid solutions for diesel soot combustion, *Chem. Commun.* 46 (2010) 457–459.
  - [22] G. Zhang, Z. Zhao, J. Xu, J. Zheng, J. Liu, G. Jiang, A. Duan, H. He, Comparative study on the preparation, characterization and catalytic performances of 3DOM Ce-based materials for the combustion of diesel soot, *Appl. Catal. B* 107 (2011) 302–315.
  - [23] D.J. Kim, Lattice parameters, ionic conductivities, and solubility limits in fluorite-structure MO<sub>2</sub> oxide [M = Hf<sup>4+</sup>, Zr<sup>4+</sup>, Ce<sup>4+</sup>, Th<sup>4+</sup>, U<sup>4+</sup>] solid solutions, *J. Am. Ceram. Soc.* 72 (1989) 1415–1421.
  - [24] M. Mogensen, A. Trovarelli (Ed.), *Catalysis by Ceria and Related Materials*, Imperial College Press, London, 2002p. 462.
  - [25] B.A.A.L. van Setten, J.M. Schouten, M. Makkee, J.A. Moulijn, Realistic contact for soot with an oxidation catalyst for laboratory studies, *Appl. Catal. B* 28 (2000) 253–257.
  - [26] C. Bueno-Ferrer, S. Parres-Escalopez, D. Lozano-Castelló, A. Bueno-López, Relationship between surface area and crystal size of pure and doped cerium oxides, *J. Rare Earths* 28 (2010) 647.
  - [27] S.I. Ahmad, P.K. Rao, I.A. Syed, Sintering temperature effect on density, structural and morphological properties of Mg-and Sr-doped ceria, *J. Taibah Univ. Sci.* 10 (2016) 381–385.
  - [28] A. Davó-Quiñonero, J. González-Mira, I. Such-Basañez, J. Juan-Juan, D. Lozano-Castelló, A. Bueno-López, Improved CO oxidation activity of 3DOM Pr-doped ceria catalysts: something other than an ordered macroporous structure, *Catal. Today* 7 (2017) 67.
  - [29] V. Alcalde-Santiago, A. Davó-Quiñonero, I. Such-Basañez, D. Lozano-Castelló, A. Bueno-López, Macroporous carrier-free Sr-Ti catalyst for NO<sub>x</sub> storage and reduction, *Appl. Catal. B* 220 (2018) 524–532.
  - [30] D. Terribile, A. Trovarelli, J. Llorca, C. de Leitenburg, G. Dolcetti, The preparation of high surface area CeO<sub>2</sub>–ZrO<sub>2</sub> mixed oxides by a surfactant-assisted approach, *Catal. Today* 43 (1998) 79–88.
  - [31] J.Z. Shyu, W.H. Weber, H.S. Gandhi, Surface characterization of alumina-supported ceria, *J. Phys. Chem.* 92 (1988) 4964–4970.
  - [32] J. Guzman, S. Carrettin, A. Corma, Spectroscopic evidence for the supply of reactive oxygen during CO oxidation catalyzed by Gold supported on nanocrystalline CeO<sub>2</sub>, *J. Am. Chem. Soc.* 127 (2005) 3286–3287.
  - [33] B. Skármán, T. Nakayama, D. Grandjean, R.E. Benfield, E. Olsson, K. Niijihara, L.R. Wallenberg, Morphology and structure of CuOx/CeO<sub>2</sub> nanocomposite catalysts produced by inert gas condensation: an HREM, EFTEM, XPS, and high-energy diffraction study, *Chem. Mater.* 14 (2002) 3686–3699.
  - [34] B. Skármán, D. Grandjean, R.E. Benfield, A. Hinz, A. Andersson, L.R. Wallenberg, Carbon monoxide oxidation on nanostructured CuOx/CeO<sub>2</sub> composite particles characterized by HREM, XPS, XAS, and high-energy diffraction, *J. Catal.* 211 (2002) 119–133.
  - [35] Mark C. Biesinger, Advanced analysis of copper X-rayphotoelectron spectra, *Surf. Interface Anal.* 49 (2017) 1325–1334.
  - [36] A. Laachir, V. Perrichon, A. Badri, J. Lamotte, E. Catherine, J.C. Lavalle, J. El Fallal, L. Hilaire, F. le Normand, E. Quémére, G.N. Sauvion, O. Touret, Reduction of CeO<sub>2</sub> by hydrogen. Magnetic susceptibility and fourier-transform infrared, ultraviolet and X-ray photoelectron spectroscopy measurements, *J. Chem. Soc. Faraday Trans.* 87 (1991) 1601–1609.
  - [37] I. Aarna, E.M. Suuberg, Review of the kinetics of the nitric oxide-carbon reaction, *Fuel* 76 (1997) 475–491.
  - [38] Y.H. Li, G.Q. Lu, V. Rudolph, The kinetics of NO and N<sub>2</sub>O reduction over coal chars in fluidised-bed combustion, *Chem. Eng. Sci.* 53 (1998) 1–26.
  - [39] T. Andana, M. Piumetti, S. Bensaid, L. Veyre, C. Thieuleux, N. Russo, D. Fino, E.A. Quadrelli, R. Pirone, CuO nanoparticles supported by ceria for NO<sub>x</sub>-assisted soot oxidation: insight into catalytic activity and sintering, *Appl. Catal. B* 216 (2017) 41–58.
  - [40] I. Atribak, A. Bueno-López, A. García-García, Combined removal of diesel soot particulates and NO<sub>x</sub> over CeO<sub>2</sub>–ZrO<sub>2</sub> mixed oxides, *J. Catal.* 259 (2008) 123–132.